Spontaneous Self-propulsion and Nonequillibrium Shape Fluctuations of a Droplet Enclosing Active Particles

Gasper Kokot
Northwestern University
Hammad Faizi
Northwestern University
Gerardo Pradillo
Northwestern University
Alexey Snezhko
Argonne National Laboratory https://orcid.org/0000-0001-5634-6228
Petia Vlahovska (petia.vlahovska@northwestern.edu)
Northwestern University https://orcid.org/0000-0001-7549-930X

Article

Keywords: Spontaneous self-propulsion, nonequillibrium shape, fluctuations, active particles, droplet, soft confinement

Posted Date: November 8th, 2021

DOI: https://doi.org/10.21203/rs.3.rs-991436/v1

Version of Record: A version of this preprint was published at Communications Physics on April 14th, 2022. See the published version at https://doi.org/10.1038/s42005-022-00872-9.

Spontaneous self-propulsion and nonequillibrium shape fluctuations of a droplet enclosing active particles

Gašper Kokot,[1,2,3] Hammad Faizi,[4] Gerardo Pradillo,[4] Alexey Snezhko,[2] and Petia M. Vlahovska[1]

[1] *Engineering Sciences and Applied Mathematics, Northwestern University, Evanston, IL 60208, USA*

[2] *Materials Science Division, Argonne National Laboratory, Lemont, IL 60439, USA*

[3] *Institute for Biophysics, Medical Faculty, University of Ljubljana, Vrazov trg 2, Ljubljana, SI-1000, Slovenia*

[4] *Mechanical Engineering, Northwestern University, Evanston, IL 60208, USA*

(Dated: October 21, 2021)

ABSTRACT

Active particles, such as swimming bacteria or self-propelled colloids, spontaneously assemble into large-scale dynamic structures. Geometric boundaries often enforce different spatio-temporal patterns compared to unconfined environment and thus provide a platform to control the behavior of active matter. Here, we report collective dynamics of active particles enclosed by soft, deformable boundaries, that is responsive to the particles' activity. We reveal that a fluid droplet enclosing motile colloids powered by the Quincke effect (Quincke rollers) exhibits strong shape fluctuations, and while the rollers do self-organize into a single vortex, it fills the droplet interior. We demonstrate that the shape fluctuations have a power spectrum consistent with active fluctuations driven by particle-interface collisions, and a broken detailed balance confirms the nonequilibrium nature of the shape dynamics. We further find that the rollers activity coupled to soft boundary fluctuations can result in a spontaneous symmetry breaking and vortex splitting. The droplet acquires motility while the vortex doublet exists. Our findings provide insights into the complex collective behavior of active colloidal suspensions in soft confinement.

INTRODUCTION

Active (self-driven) particles such as motile colloids present novel opportunities for the engineering of smart materials that can self–heal or change properties on demand [1]. The reconfigurability of active materials stems from the propensity of active particles to self-organize into large-scale dynamic structures that can be modulated by external cues such as electric or magnetic fields [2–9], light [10, 11], or chemical reactions [12–14]. The spatio-temporal patterns can be also manipulated by geometric boundaries. For example, while unconfined suspensions of bacteria exhibit turbulent-like flow [15–18], confinement into a long and narrow macroscopic "racetrack" geometry stabilizes bacterial motion into a steady unidirectional circulation [19, 20], and when subjected to 2D arrays of vertical pillars arranged in a square pattern bacterial suspensions transforms into a lattice of hydrodynamically bound vortices with a long-range antiferromagnetic order [21]. Inside of a droplet, the bacteria form a macro-scale bidirectional vortex [22, 23]. Similar behaviors are also observed with synthetic microswimmers. For example, the Quincke rollers, which are powered by a spontaneous electro-rotation of a dielectric sphere exposed to a static electric field, self-organize into a long, polar band and undergo directional motion in the racetrack microfluidic channel [24], while in strong confinement (rectangular geometries), the band state is replaced by a single macroscopic vortex [25].

A confinement that is responsive to the particles activity adds another degree of freedom that can unlock novel collective dynamic states. Active particles encapsulated in a droplet or a vesicle (bilayer membrane sac) drive strong shape deformations [26–29] and can cause net motion [26, 30–33]. Here, we explore the relation between the particle's activity, deformations and motility of the soft confining container. As active particles we employ the Quincke rollers since their speed and locomotion pattern can be easily manipulated [34, 35]. We use a soft container comprised of a liquid droplet sandwiched between two electrodes, which creates quasi two-dimensional geometry. We find that at low activity (quantified by the speed of the rollers) the droplet contour fluctuates, while the droplet stays nearly stationary, and the rollers self-organize into a vortex spanning the whole system. Increasing the activity leads to a growth of the shape fluctuations that exhibit a power spectrum consistent with active fluctuations driven by particle-interface collisions. Coupling of activity and soft boundary fluctuations often results in bursts of the droplet translation in a randomly selected direction. The net propulsion is driven by a spontaneous formation of a vortex doublet composed of two counter-rotating vortices.

RESULTS

Particle dynamics inside the droplet

The experimental system consists of 40 µm polystyrene spheres dispersed in hexadecane/AOT media (see Methods for details). A small volume of the solution (approx. 5 µL) is sandwiched between two indium tin oxide (ITO) coated glass electrodes spaced 150 µm apart to form a liquid bridge with a high aspect ratio that produces a quasi-two-dimensional droplet (Fig.1a). The particles are allowed to sediment on the bottom electrode before the application of a uniform DC electric field E between the electrodes. Above a threshold magnitude E_Q particles develop a steady rotation due to the Quincke effect [24, 36] (see SI) and start to roll in the presence of the bottom surface. The rollers generate hydrodynamic flows that promote alignment of their translational directions and result in a formation of multiple transient flocks and vortices of particles (Fig. 1bc).

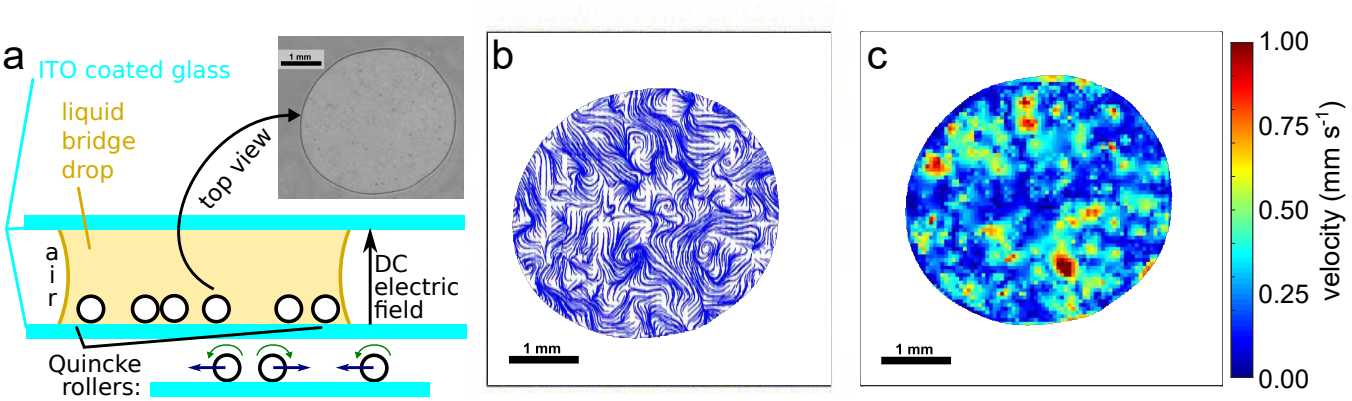

FIG. 1. Quincke rollers in a droplet. (a) A sketch of the experimental system: A small amount of weakly conductive liquid (hexadecane) surrounded by air forms a bridge between two planar electrodes. Inside of the quasi-two-dimensional drop are polystyrene spheres that start to roll upon application of a uniform DC electric field, E. Quincke rollers initially move in random directions along the surface of the bottom electrode. The image shows the top view of the drop and enclosed rollers. (b) The rollers stir the fluid and generate strong flow. Streamlines reveal the formation of transient vortices throughout the droplet. (c) Snapshot of the velocity field inside the droplet as determined by particle image velocimetry (PIV). Experimental parameters: packing fraction of the Quincke rollers $\varphi = 0.58 \pm 0.11$, droplet area is $A_{drop} = 11.05 \pm 0.03\,\mathrm{mm}^2$, the driving electric field $E = 3.193 \pm 0.007\,\mathrm{MV\,m}^{-1}$.

Eventually, multiple vortices and flocks merge to form a macroscopic global vortex inside the droplet, see Fig. 2b,c. Similarly to vortices formed by magnetic rollers [37, 38], the vortex spontaneously selects its handedness (clockwise or counterclockwise) that changes from experiment to experiment. The particles velocity fields in the droplet reveal a dramatic change in its appearance compared to rollers confined by a solid boundary [25], where the rollers accumulate near the confining interface. In the droplet system, the rollers are distributed throughout the droplet interior being more packed in the center of the droplet and less densely packed towards the drop edge. This is most clearly seen in Fig. 2c as one bright blur in the center of the droplet - a big crowd of rollers rotating as one vortex - and several bright blurs around - flocks orbiting in the direction of the rotation. Equal direction of rotation for the whole system is confirmed by a single central peak in the vorticity field of Fig. 2c. For comparison, in Fig. 2b, where the system is in the intermediate state, there are several large off-center bright blurs - crowds of rollers creating vortical flows with clock or counter-clock wise as illustrated by the local minima and a maxima in the vorticity field of Fig. 2b. For a closer inspection see SI Video 2.

The equilibrium droplet contour in the absence of activity (below the onset of Quincke rotation) is a circle (Fig. 2a). Once the rollers become motile, the interface begins to fluctuate and during the process of vortex formation the droplet shape can become very non-circular (see Fig. 2b and SI Video 1). Once the vortex is formed the shape deviations from a circle becomes negligible (see Fig. 2c and SI Video 2). We quantify the droplet deformations by the asphericity parameter Δ (see Methods), with $\Delta = 0$ corresponding to a perfect circle. Fig. 2d shows that once the system is energized, the droplet undergoes pronounced shape deformations until a macroscopic vortex is formed and Δ decreases back to nearly pre-activation values (nevertheless shape fluctuations are still present). The gradual growth of the macroscopic vortex is illustrated by a correlation length, r_{corr}, defined as the first zero crossing of the spatial velocity correlation function, $C_{norm}(r)$ (Fig. 2d inset). r_{corr} exhibits a monotonic growth while the individual rollers organize into flocks and transient vortices, and it reaches a plateau when the globally correlated state (vortex) is formed.

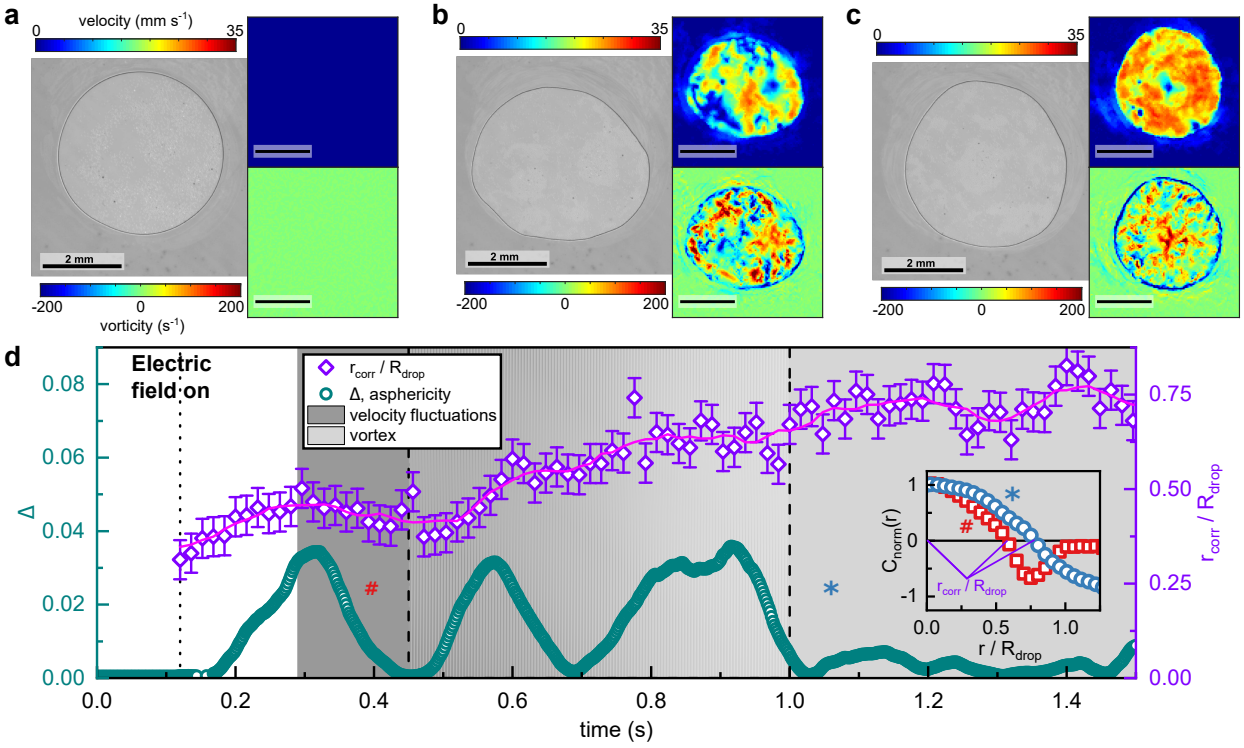

FIG. 2. Shape fluctuations of a droplet with Quincke rollers. (a)A droplet in the absence of the electric field, $E = 0$. (b) Regime of transient flocks and vortices. Rollers velocity (top right) and vorticity (bottom right) fields in the droplet. Both clockwise (blue) and counter-clockwise (red) vorticity is simultaneously present indicative of transient vortices. (c) Globally correlated state. Velocity(top right) and vorticity (bottom right) fields indicate the presence of a single macroscopic vortex. (d) Evolution of the droplet shape characterized by the asphericity, Δ (cyan circles, left scale). The right scale presents the time evolution of the correlation length r_{corr} on the same dataset, as defined in the inset from $C_{norm}(r)$, the normalized spatial correlation of velocity field, first zero crossing, normalized by the drop radius R_{drop}. The inset shows $C_{norm}(r)$ computed from the data in the gray-shaded regions. Experimental parameters: $\varphi = 0.18 \pm 0.04$, $A_{drop} = 13.56 \pm 0.03\,\mathrm{mm}^2$ and $E = 5.104 \pm 0.008\,\mathrm{MV\,m}^{-1}$.

Nonequillibrium shape fluctuations

The shape of the active droplet exhibits strong fluctuations with amplitude reaching $10-15\%$ of the initial droplet radius, see Fig. 3a. The power spectrum of the shape fluctuations exhibits dependence on wavenumber q, $\langle |h(q)|^2 \rangle \sim q^{-4}$ (Fig. 3b). Thermal fluctuations of the droplet interface would exhibit a power spectrum with q^{-2} capillary scaling for surface-tension-controlled shape relaxation, suggestive that the origin of the fluctuations is non-equilibrium.

To confirm the non-equilibrium nature of the fluctuations, we test for broken detailed balance in the transitions between microscopic configurations [39] (see Methods). The configurations correspond to the shapes defined by different Fourier modes. In equilibrium, it is equally likely for the forward and backward transition to occur between any two different Fourier modes. A non-equilibrium system, however, would display a probability flux in the phase space of shapes. Fig. 3c shows the probability density map for two Fourier modes of the fluctuating droplet.The probability is defined as the ratio of the time spent at a given state. The arrows indicate the currents across box boundaries determined by counting transitions between boxes. Computing the contour integral of the probability current, $\Omega = \frac{\oint_C \mathbf{j}\cdot d\mathbf{l}}{\oint_C |\mathbf{j}|\, dl}$, shows a non-zero circulation, confirming that the system is out of equilibrium.

Intriguingly, in the active state, the relaxation time obtained from the time autocorrelation function, $\langle h_q(0)\, h_q^*(t) \rangle = \langle |h_q|^2 \rangle \exp(-\frac{t}{\tau_q})$, displays a power-law decay close to q^{-1}, see Fig. 3d. In equilibrium systems, thermal fluctuations with mean-squared amplitude $\sim q^4$ (as in bilayer membranes) show q^{-3} relaxation rates [29]. However, in non-equilibrium systems the excitation and relaxation need not to have same driving forces. In our system, the fluctuations are driven by the strong flows generated by the Quincke rollers. Indeed, the q^{-4}-law of the power spectrum is consistent

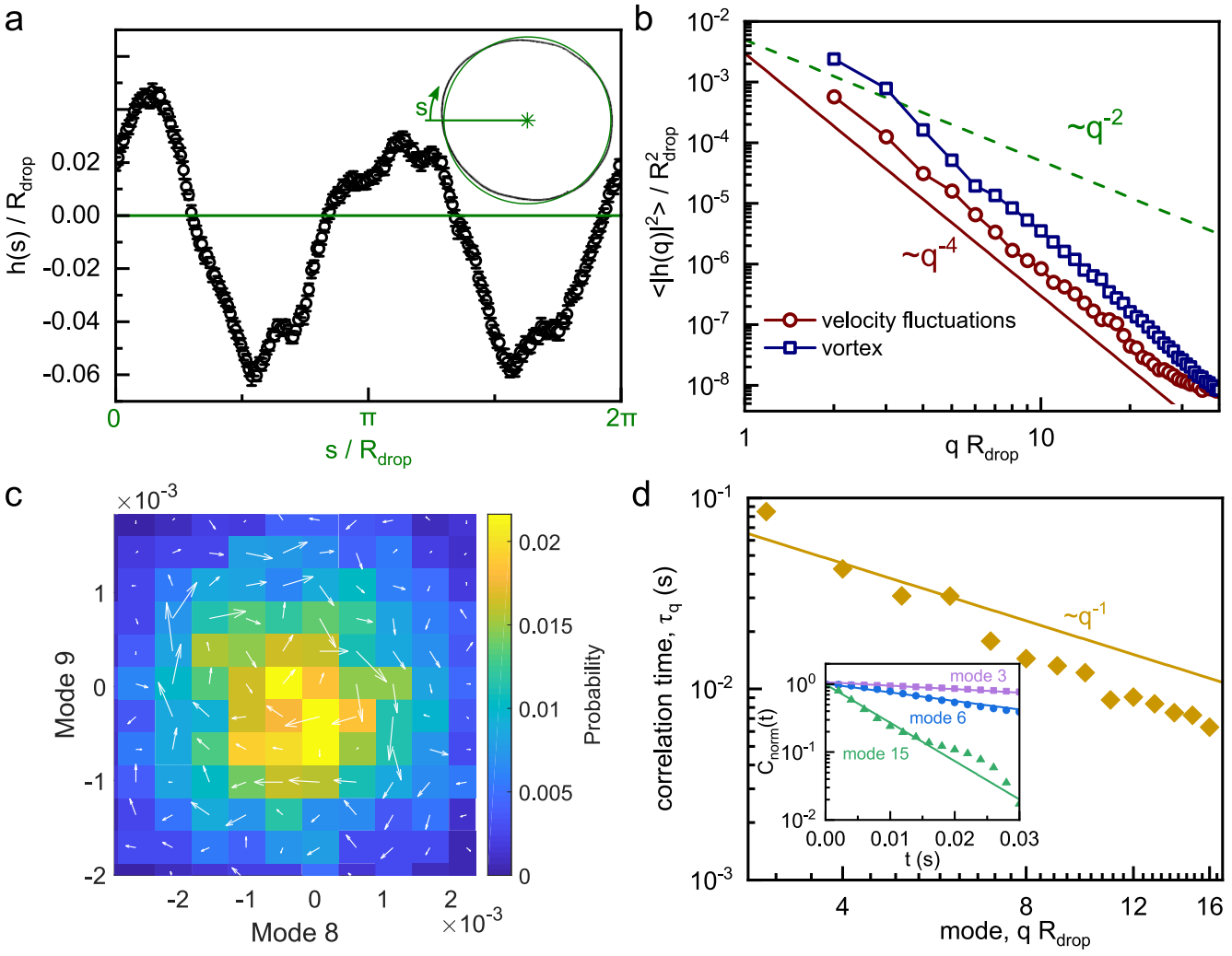

FIG. 3. (a) A snapshot of the contour h around the equivalent circle radius R_{drop}. The coordinate s runs along the circumference of the equivalent circle (inset, green). The liquid-air interface is deformed (inset, black) by the activity inside the droplet and deviates from R_{drop} by h. (b) An example time averaged power spectrum $\langle|h(q)|^2\rangle$ dependence on the wave number $q = 2\pi/(sR_{drop})$ for two cases: fluctuating velocity regime ($\varphi = 0.58\pm0.11$, $A_{drop} = 11.05\pm0.08\,\mathrm{mm}^2$ and $E = 3.193\pm0.007\,\mathrm{MV\,m^{-1}}$) and fully developed vortex regime ($\varphi = 0.18\pm0.04$, $A_{drop} = 13.56\pm0.03\,\mathrm{mm}^2$ and $E = 5.104\pm0.008\,\mathrm{MV\,m^{-1}}$). In both cases the decay of the power spectrum clearly falls off as q^{-4}. (c) Probability distribution (color) and flux map (arrows) in phase space spanned by Fourier modes 8 and 9. Arrows length corresponds to the magnitude of the fluxes. More plots are available in the SI. The contour integral of the probability current, $\Omega = \frac{\oint_C \mathbf{j}\cdot d\mathbf{l}}{\oint_C |\mathbf{j}|\ dl} = -0.59\pm0.11$. (d) Relaxation time of the autocorrelations as a function of the wavenumber q. The inset shows the autocorrelation functions for 3 modes .

with active shape fluctuations due to particle-interface collisions [29]. The deformations are opposed by the surface tension and the relaxation rates are set by dissipation due to the motion of the contact line [40, 41]. An estimate based on the balance of surface tension γ and viscous dissipation by viscosity μ gives for the relaxation time $\tau_q = \mu/\gamma\theta^3 q$, where θ is the contact angle [40]. Using the values for our experimental system, $\mu = 1\,\mathrm{mPa\,s}$ and surface tension $\gamma = 10\,\mathrm{mN\,m^{-1}}$, and estimating the contact angle to be $\theta \sim 1$ yields $\tau_q \sim 0.1/(qR_{drop})$ in good order of magnitude agreement with the experimentally measured values.

Activity enhancement of the shape fluctuations

Thermally-driven droplet shape fluctuations are negligible in our system due to strong surface tension. For an oil/air interface the surface tension is $\gamma = 10\,\mathrm{mN\,m^{-1}}$, which corresponds to interfacial energy far exceeding the thermal

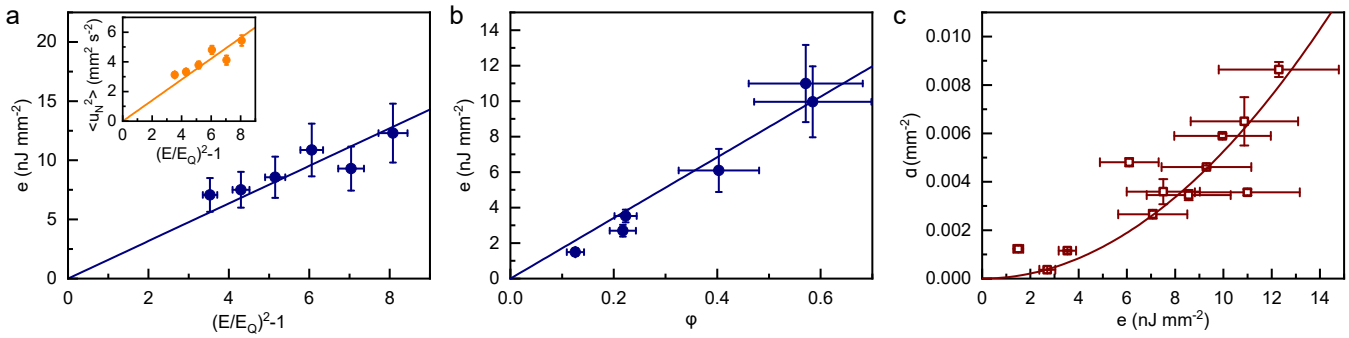

FIG. 4. (a) The energy per area, e, dependence on $(E/E_Q)^2-1$, with $E_{onset} = 1.50\pm0.03\,\mathrm{MV\,m^{-1}}$. Inset: Linear dependence of the square average of velocity fluctuations $\langle u_N^2\rangle$ on $(E/E_Q)^2-1$. In both cases the line is a least squares fit to the experimental points. All experiments were performed on the same liquid bridge bubble with $\varphi = 0.58\pm0.11$ and $A_{drop} = 11.05\pm0.03\,\mathrm{mm^2}$. (b) As predicted by Eq. 2, the energy density e is linearly dependent on φ. The line is a least squares fit to the experimental points. All experiments were performed at the same $E = 4.25\pm0.01\,\mathrm{MV\,m^{-1}}$, each liquid bridge bubble was prepared separately with A_{drop} in the range from $8.97\,\mathrm{mm^2}$ to $11.25\,\mathrm{mm^2}$. (c) A graph of the power spectrum slope α: $\langle|h(q)|^2\rangle = \alpha q^{-4}$ versus e demonstrates a quadratic dependence (red line). The experimental points were obtained from several realizations of Quincke rollers inside a liquid bridge covering the ranges: E from $3.19\,\mathrm{MV\,m^{-1}}$ to $4.52\,\mathrm{MV\,m^{-1}}$; φ from 0.13 to 0.58; and A_{drop} from $8.97\,\mathrm{mm^2}$ to $11.25\,\mathrm{mm^2}$.

energy, $\sim 10^{12}k_BT$, for a droplet with radius of 1 mm. However, in the active state the rollers generate flows that can be strong enough to overcome surface tension and deform the interface. An individual roller with radius a moves with speed $a\dot{G}$, where the generated flow strain rate is $\dot{G} = \tau_{\mathrm{mw}}^{-1}\sqrt{(E/E_Q)^2-1}$ (see SI for details). In our system, the Maxwell-Wagner time is $\tau_{\mathrm{mw}} \sim 1\,\mathrm{ms}$. The flow can extert stress on the interface in the order of $\mu\dot{G} \sim 1\,\mathrm{Pa}$, which is comparable to the capillary stress γ/R_{drop}. Since the flow is created by the rollers, the active shape fluctuations are expected to increase if either the rollers velocity or number increases.

To quantify the effects of the activity, we define an effective energy of the system from velocity fluctuations [42]

$$U = \frac{1}{2}\sum_N m_N u_N^2 \tag{1}$$

where the index N runs over the individual rollers, and $\mathbf{u_N} = \mathbf{v_N} - \mathbf{v}$ is the difference between the individual roller velocity, $\mathbf{v_N}$, the macroscopic flow, $\mathbf{v}$. Experimentally, however, we have access neither to the individual particle trajectories nor the detailed hydrodynamic flow, therefore we consider $\mathbf{v}$ to be the instantaneous velocity of the droplet center and $\mathbf{v_N}$ the velocity field pixel from PIV velocity fields of the particles. PIV procedure is based on image contrast correlations and detects only the movement of the particles in the droplet making the velocity field a good approximation for the actual particle velocities as long as the packing fraction φ is large. Assuming that all particles have equal mass $m_N = m_p$ and replacing the summation by the temporal average value of the square of the velocity fluctuations $\langle u_N^2\rangle$ yields for the energy density

$$e = U/A_{droplet} = \frac{2}{3}\varphi a\rho\langle u_N^2\rangle, \tag{2}$$

where ρ is the buoyant density of particles. In our system the velocity of individual particles depends on the driving electric field E [24, 43], thus we have an external control over the velocity fluctuations. The $\langle u_N^2\rangle$ linearly increases with $(E/E_Q)^2-1$ (see Fig. 4a inset) and, as a result, the energy density e is proportional to $(E/E_Q)^2-1$ (Fig. 4a). The energy density also follows a linear dependence on the packing fraction φ as predicted by Eq. [2] (Fig. 4b), demonstrating that addition of active agents is directly reflected in increased energy injection into the droplet.

The magnitude of the active shape fluctuations scales as $\langle|h(q)|^2\rangle = \alpha q^{-4}$ (Fig. 3b) consistent with the theoretical model for fluctuations due to particle collisions with a fluid interface governed by surface tension [29]. The theoretical model also predicts that the power spectrum should increase quadratically with the active pressure. Given that the pressure is the volumetric energy density, the theory thus suggests that α should scale quadratically with the energy density, which is in agreement with our experimental results (Fig. 4c).

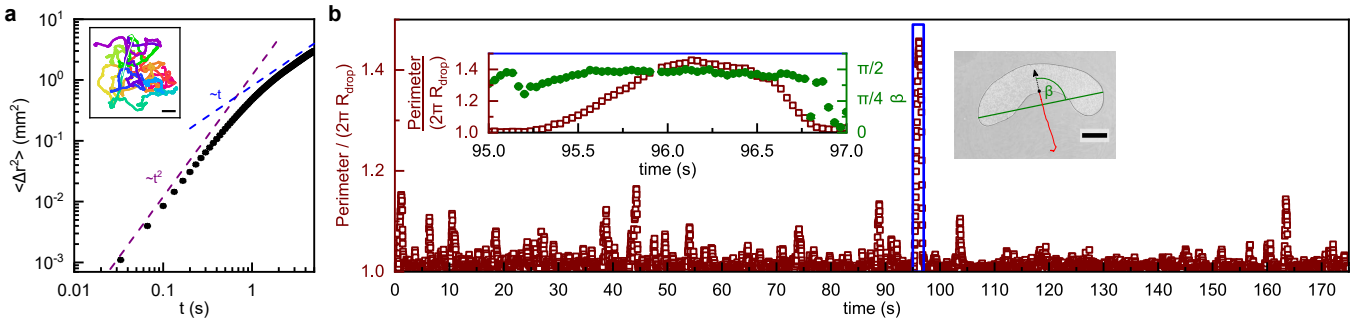

FIG. 5. (a) An example of the experimental mean square displacement for the drop center of mass (MSD) $\langle \Delta r^2 \rangle$. Inset: Trajectory of the droplet center of mass for the duration of experiment. The color progression from red to violet indicates the passage of time, the white line is a part of the trajectory that is featured in the blowout of (b). Scale bar is 1 mm. (b) Time series for the droplet perimeter normalized by the equivalent circle perimeter shows surges in droplet deformation accompanied by directed motion. Inset: A closer inspection reveals that the direction of motion is perpendicular to the maximal caliper diameter defined with an angle β (see inset snapshot, the green line is the obtained maximal caliper (Feret) diameter and the red line is the trajectory up to that moment, Scale bar is 1 mm). Experimental parameters: $\varphi = 0.28 \pm 0.02$, $A_{drop} = 10.07 \pm 0.03\,\mathrm{mm}^2$, $E = 4.464 \pm 0.008\,\mathrm{MV\,m}^{-1}$.

Spontaneous droplet self-propulsion

The shape fluctuations are accompanied by a motion of the droplet as a whole. The behavior of the mean square displacement (MSD) $\langle \Delta r^2 \rangle$ for the center of the droplet exhibits a typical diffusive behavior at the long time scales (see Fig. 5a), and it is in agreement with the behavior observed with droplets enclosing bacteria [32] or active nematics [**?**], and predicted by simulations for microswimmers in a vesicle [26]. As activity increases, the droplet shape fluctuations grow and the system occasionally undergoes a symmetry-breaking instability. The global vortex spontaneously splits into two counter-rotating entities that drive a significant elongation of the droplet (as illustrated by the changes in the droplet perimeter shown in Fig. 5b and SI Video 3) along the line connecting the centers of the new vortices. Such events result in bursts of persistent motion of the droplet in a randomly chosen direction reminiscent of the Levy flights. During the vortex pair formations the maximal Feret diameter of the droplet is always perpendicular to the direction of the droplet travel (corresponding angle to $\beta \approx \pi/2$), see the inset of Fig. 5b) in contrast to the regular droplet excursions that do not show correlations between β and velocity of the droplet (see SI Fig. S1). The droplet translation persist for about $2 - 3\,\mathrm{s}$ after which the vortex pair recombines into the global vortex and the droplet restores its nearly-circular shape. The events of spontaneous splitting of the self-assembled vortex into two entities leading to a droplet elongation and subsequent bursts of self-propulsion are probabilistic and statistically rare compared to the regular behavior but the phenomenon is robust.

DISCUSSION

In this work we experimentally explored the dynamics of motile colloids in soft confinement. We employ Quincke rollers in a droplet as a model system, with the rollers speed easily controlled by the applied field strength. We find that the interplay between deformable confinement and activity-driven flow gives rise to several previously unobserved phenomena. At low activity, the rollers form a vortex spanning the whole droplet, in contrast to rollers in solid-wall confinement, where the particles accumulate near the boundary. The droplet contour fluctuates about a circular shape and the fluctuations power spectrum is consistent with active fluctuations driven by particle-interface collisions. The non-equilibrium nature of the shape fluctuations is revealed by a broken detailed balance of the shape dynamics. While the interface deformation is driven by the particle-induced flow, the relaxation is controlled by surface tension as evidenced by the time correlations of the shape fluctuations. Shape fluctuations grow with the activity and can result in a spontaneous extension of the droplet in one direction driven by a formation of the vortex doublet. The spontaneous droplet elongations are accompanied by bursts of persistent self-propulsion in a direction perpendicular to the extension axis. The vortex splitting and recovery lasts for few seconds during which time the droplet can travel a distance of several droplet radii. The timing of the excursion and the direction of motion are randomly chosen. Their control requires understanding of the symmetry-breaking mechanism that leads to the vortex doublet formation. Our results provide insights into the complex dynamic behavior of active colloidal suspensions confined by a deformable boundary and provide new directions for future research in the engineering of self-propelled micromachines.

METHODS

Experimental system

Spherical polystyrene particles ($d = 2a = 40\,\mu m$ diameter, Phosphorex) and density $1.06\,g\,cm^{-3}$ in hexadecane ($\rho_{hexadecane} = 0.77\,g\,cm^{-3}$) are dispersed in hexadecane with $0.1\,mol\,L^{-1}$ dioctyl sulfosuccinate sodium (AOT) salt (Sigma Aldrich). A small amount of the solution with the particles (approx. $5\,\mu L$) is sandwiched between two indium tin oxide (ITO) coated glass slides to form a liquid bridge with a high aspect ratio. The distance between the electrodes is set by glass spheres with diameter$150\,\mu m$ (Novum Glass) embedded in vacuum grease. Particles are allowed to sediment on the bottom electrode. We explore several packing fractions φ, ranging from 0.13 to 0.58, of Quincke rollers inside droplets.

Imaging and droplet shape analysis

The recordings are made with a fast CMOS camera (IDT) at 300 fps and 500 fps mounted on a stereoscope (Leica). Velocity, vorticity fields and streamlines reflect the motion of the Quincke rollers and were obtained by a particle image velocimetry (PIV) package MatPIV for Matlab. Velocity fields together with the movement of the entire liquid bridge served as the input to calculate the energy per unit area E_{tot}/A_{drop} of the system.

To characterize the droplet contour fluctuations each image was automatically thresholded by Otsu's method in Matlab to obtain the border outline. The center of the droplet $\vec{R_c}$ was determined as the mean coordinates of the droplet area pixels, A_{drop}, and equivalent radius was calculated $R_{drop} = \sqrt{A_{drop}/\pi}$. The perimeter of the equivalent circle with R_{drop} around $\vec{R_c}$ served as the baseline for the coordinate r and the radial deviations form the equivalent circle $h(r)$ were determine from the images (Fig. 3a inset). We used the square of the fast Fourier transform algorithm in Matlab to compute the power spectrum of the fluctuations and averaged it over time. The number of frames to calculate the temporal averages of all the measured quantities was > 2000, errors represent the standard error of the mean value.

The droplet radius of gyration R_g and asphericity Δ were determined by the gyration tensor $\overline{\overline{Q}} = \frac{1}{N}\sum_{n=1}^{N}(\vec{R_n} - \vec{R_c}) \otimes (\vec{R_n} - \vec{R_c})$, where index n runs over all area pixels of the liquid bridge drop (N in total). $\overline{\overline{Q}}$ has eigenvalues λ_1 and λ_2 which define $R_g = \sqrt{\lambda_1 + \lambda_2}$ and $\Delta = (\lambda_1 - \lambda_2)^2/(\lambda_1 + \lambda_2)^2$.

Detailed balance analysis of the shape fluctuations

The methodology follows Ref. [39] to analyze the transitions between microscopic configurations defined as the shapes corresponding to different Fourier modes. We compute the trajectory in the phase space spanned by the two modes from the time series of their amplitudes. Then the phase space is discretized into equally sized, rectangular boxes each of which represents a discrete state. The probability is defined as the ratio of the time spent at a given state and the total trajectory time. The arrows indicate the currents across box boundaries determined by counting transitions between boxes. The transitions between neighboring discrete states occur when the system trajectory crosses box boundaries. Computing the contour integral of the probability current, $\Omega = \frac{\oint_C \mathbf{j}\cdot d\mathbf{l}}{\oint_C |\mathbf{j}|\ dl}$, shows a non-zero circulation for a system is out of equilibrium. Details of the methodology can be found in SI.

[1] Gerhard Gompper, Roland G Winkler, Thomas Speck, Alexandre Solon, Cesare Nardini, Fernando Peruani, Hartmut Löwen, Ramin Golestanian, U Benjamin Kaupp, Luis Alvarez, et al. The 2020 motile active matter roadmap. *Journal of Physics: Condensed Matter*, 32(19):193001, 2020.

[2] Alexey Snezhko and Igor S Aranson. Magnetic manipulation of self-assembled colloidal asters. *Nature materials*, 10(9): 698–703, 2011.

[3] A Van Blaaderen, M Dijkstra, RHHG van Roij, A Imhof, M Kamp, BW Kwaadgras, T Vissers, and B Liu. Manipulating the self assembly of colloids in electric fields. *The European Physical Journal Special Topics*, 222(11):2895–2909, 2013.

[4] Jure Dobnikar, Alexey Snezhko, and Anand Yethiraj. Emergent colloidal dynamics in electromagnetic fields. *Soft Matter*, 9(14):3693–3704, 2013.

[5] Jing Yan, Ming Han, Jie Zhang, Cong Xu, Erik Luijten, and Steve Granick. Reconfiguring active particles by electrostatic imbalance. *Nature materials*, 15(10):1095–1099, 2016.

[6] Koohee Han, C Wyatt Shields IV, and Orlin D Velev. Engineering of self-propelling microbots and microdevices powered by magnetic and electric fields. *Advanced Functional Materials*, 28(25):1705953, 2018.

[7] Koohee Han, Gašper Kokot, Oleh Tovkach, Andreas Glatz, Igor S Aranson, and Alexey Snezhko. Emergence of self-organized multivortex states in flocks of active rollers. *Proceedings of the National Academy of Sciences*, 117(18):9706–9711, 2020.

[8] Michelle Driscoll and Blaise Delmotte. Leveraging collective effects in externally driven colloidal suspensions: Experiments and simulations. *Current opinion in colloid & interface science*, 40:42–57, 2019.

[9] Koohee Han, Gašper Kokot, Shibananda Das, Roland G Winkler, Gerhard Gompper, and Alexey Snezhko. Reconfigurable structure and tunable transport in synchronized active spinner materials. *Science advances*, 6(12):eaaz8535, 2020.

[10] Jeremie Palacci, Stefano Sacanna, Asher Preska Steinberg, David J Pine, and Paul M Chaikin. Living crystals of light-activated colloidal surfers. *Science*, 339(6122):936–940, 2013.

[11] Hanumantha Rao Vutukuri, Maciej Lisicki, Eric Lauga, and Jan Vermant. Light-switchable propulsion of active particles with reversible interactions. *Nature communications*, 11(1):1–9, 2020.

[12] Walter F Paxton, Kevin C Kistler, Christine C Olmeda, Ayusman Sen, Sarah K St. Angelo, Yanyan Cao, Thomas E Mallouk, Paul E Lammert, and Vincent H Crespi. Catalytic nanomotors: autonomous movement of striped nanorods. *Journal of the American Chemical Society*, 126(41):13424–13431, 2004.

[13] Jonathan R Howse, Richard AL Jones, Anthony J Ryan, Tim Gough, Reza Vafabakhsh, and Ramin Golestanian. Self-motile colloidal particles: from directed propulsion to random walk. *Physical review letters*, 99(4):048102, 2007.

[14] Mihail N Popescu, William E Uspal, Alvaro Domínguez, and Siegfried Dietrich. Effective interactions between chemically active colloids and interfaces. *Accounts of chemical research*, 51(12):2991–2997, 2018.

[15] Christopher Dombrowski, Luis Cisneros, Sunita Chatkaew, Raymond E Goldstein, and John O Kessler. Self-concentration and large-scale coherence in bacterial dynamics. *Physical review letters*, 93(9):098103, 2004.

[16] Andrey Sokolov, Igor S Aranson, John O Kessler, and Raymond E Goldstein. Concentration dependence of the collective dynamics of swimming bacteria. *Physical review letters*, 98(15):158102, 2007.

[17] Henricus H Wensink, Jörn Dunkel, Sebastian Heidenreich, Knut Drescher, Raymond E Goldstein, Hartmut Löwen, and Julia M Yeomans. Meso-scale turbulence in living fluids. *Proceedings of the National Academy of Sciences*, 109(36): 14308–14313, 2012.

[18] Jörn Dunkel, Sebastian Heidenreich, Knut Drescher, Henricus H Wensink, Markus Bär, and Raymond E Goldstein. Fluid dynamics of bacterial turbulence. *Physical review letters*, 110(22):228102, 2013.

[19] Hugo Wioland, Francis G Woodhouse, Jörn Dunkel, and Raymond E Goldstein. Ferromagnetic and antiferromagnetic order in bacterial vortex lattices. *Nature physics*, 12(4):341–345, 2016.

[20] Maxime Theillard, Roberto Alonso-Matilla, and David Saintillan. Geometric control of active collective motion. *Soft Matter*, 13:363–375, 2017. doi:10.1039/C6SM01955B. URL `http://dx.doi.org/10.1039/C6SM01955B`.

[21] Daiki Nishiguchi, Igor S Aranson, Alexey Snezhko, and Andrey Sokolov. Engineering bacterial vortex lattice via direct laser lithography. *Nature communications*, 9(1):1–8, 2018.

[22] Hugo Wioland, Francis G Woodhouse, Jörn Dunkel, John O Kessler, and Raymond E Goldstein. Confinement stabilizes a bacterial suspension into a spiral vortex. *Physical review letters*, 110(26):268102, 2013.

[23] Enkeleida Lushi, Hugo Wioland, and Raymond E Goldstein. Fluid flows created by swimming bacteria drive self-organization in confined suspensions. *Proceedings of the National Academy of Sciences*, 111(27):9733–9738, 2014.

[24] Antoine Bricard, Jean-Baptiste Caussin, Nicolas Desreumaux, Olivier Dauchot, and Denis Bartolo. Emergence of macroscopic directed motion in populations of motile colloids. *Nature*, 503(7474):95–98, 2013.

[25] Antoine Bricard, Jean-Baptiste Caussin, Debasish Das, Charles Savoie, Vijayakumar Chikkadi, Kyohei Shitara, Oleksandr Chepizhko, Fernando Peruani, David Saintillan, and Denis Bartolo. Emergent vortices in populations of colloidal rollers. *Nature communications*, 6(1):1–8, 2015.

[26] Matteo Paoluzzi, Roberto Di Leonardo, M Cristina Marchetti, and Luca Angelani. Shape and displacement fluctuations in soft vesicles filled by active particles. *Scientific reports*, 6:34146, 2016.

[27] Yao Li and Pieter Rein ten Wolde. Shape transformations of vesicles induced by swim pressure. *Physical review letters*, 123(14):148003, 2019.

[28] Hanumantha Rao Vutukuri, Masoud Hoore, Clara Abaurrea-Velasco, Lennard van Buren, Alessandro Dutto, Thorsten Auth, Dmitry A Fedosov, Gerhard Gompper, and Jan Vermant. Active particles induce large shape deformations in giant lipid vesicles. *Nature*, 586(7827):52–56, 2020.

[29] Sho C Takatori and Amaresh Sahu. Active contact forces drive nonequilibrium fluctuations in membrane vesicles. *Physical Review Letters*, 124(15):158102, 2020.

[30] Jiamin Chen, Yunfeng Hua, Yangwei Jiang, Xiaolin Zhou, and Linxi Zhang. Rotational diffusion of soft vesicles filled by chiral active particles. *Scientific reports*, 7(1):1–12, 2017.

[31] Clara Abaurrea-Velasco, Thorsten Auth, and Gerhard Gompper. Vesicles with internal active filaments: self-organized propulsion controls shape, motility, and dynamical response. *New Journal of Physics*, 21(12):123024, 2019.

[32] Gabriel Ramos, María Luisa Cordero, and Rodrigo Soto. Bacteria driving droplets. *Soft Matter*, 16:1359–1365, 2020. doi:10.1039/C9SM01839E. URL `http://dx.doi.org/10.1039/C9SM01839E`.

[33] Mojtaba Rajabi, Hend Baza, Taras Turiv, and Oleg D. Lavrentovich. Directional self-locomotion of active droplets enabled by nematic environment. *NATURE PHYSICS*, 17(2):260+, FEB 2021. doi:10.1038/s41567-020-01055-5.

[34] Hamid Karani, Gerardo E Pradillo, and Petia M Vlahovska. Tuning the random walk of active colloids: From individual run-and-tumble to dynamic clustering. *Physical review letters*, 123(20):208002, 2019.

[35] Bo Zhang, Andrey Sokolov, and Alexey Snezhko. Reconfigurable emergent patterns in active chiral fluids. *NATURE COMMUNICATIONS*, 11(1), SEP 2 2020. ISSN 2041-1723. doi:10.1038/s41467-020-18209-x.
[36] AO Tsebers. Internal rotation in the hydrodynamics of weakly conducting dielectric suspensions. *Fluid Dynamics*, 15(2): 245–251, 1980.
[37] Gašper Kokot and Alexey Snezhko. Manipulation of emergent vortices in swarms of magnetic rollers. *Nature communications*, 9(1):1–7, 2018.
[38] Y Wang, S Canic, G Kokot, A Snezhko, and IS Aranson. Quantifying hydrodynamic collective states of magnetic colloidal spinners and rollers. *Physical Review Fluids*, 4(1):013701, 2019.
[39] Christopher Battle, Chase P Broedersz, Nikta Fakhri, Veikko F Geyer, Jonathon Howard, Christoph F Schmidt, and Fred C MacKintosh. Broken detailed balance at mesoscopic scales in active biological systems. *Science*, 352(6285):604–607, 2016.
[40] Pierre-Gilles De Gennes. Wetting: statics and dynamics. *Reviews of modern physics*, 57(3):827, 1985.
[41] T Ondarcuhu and M Veyssié. Relaxation modes of the contact line of a liquid spreading on a surface. *Nature*, 352(6334): 418–420, 1991.
[42] Isaac Goldhirsch. Introduction to granular temperature. *Powder Technology*, 182(2):130–136, 2008.
[43] Gerardo E Pradillo, Hamid Karani, and Petia M Vlahovska. Quincke rotor dynamics in confinement: rolling and hovering. *Soft matter*, 15(32):6564–6570, 2019.
[44] Tong Gao and Zhaorui Li. Self-driven droplet powered by active nematics. *Phys. Rev. Lett.*, 119:108002, Sep 2017. doi:10.1103/PhysRevLett.119.108002. URL `https://link.aps.org/doi/10.1103/PhysRevLett.119.108002`.

ACKNOWLEDGEMENTS

The research of A.S. and G.K. were supported by the U.S. Department of Energy, Office of Science, Basic Energy Sciences, Materials Sciences and Engineering Division. G.K. was also supported by P.M.V, H.F., G.P. were supported by NSF-DMR award 2004926.

AUTHOR CONTRIBUTIONS

A.S., P.M.V. and G.K. designed the research. G.K. performed the experiments and analyzed the data. H.F. performed the analysis of the shape fluctuations. G.P. obtained the preliminary results and discovered the crawling drop phenomenon. A.S., H.F., P.M.V and G.K. wrote the paper.

COMPETING INTEREST

There are no competing interests to declare.

Supplementary Files

This is a list of supplementary files associated with this preprint. Click to download.

- SI.pdf
- SIVideo1BorderFluctuation1.avi
- SIVideo2VortexDevelopment2.avi
- SIVideo3TravelDroplet1.avi